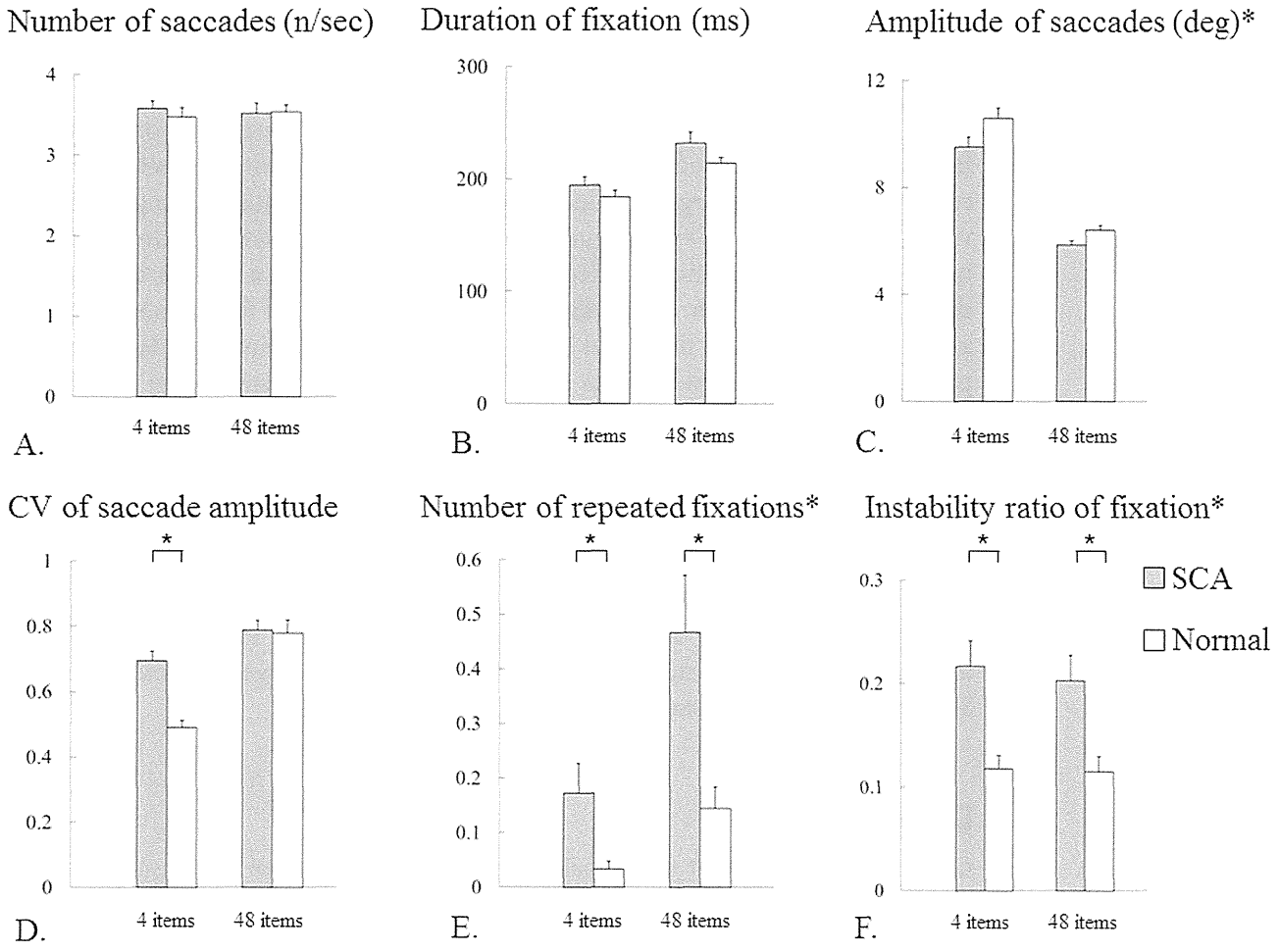

Fig. 9. Visual scanning parameters in serial search tasks. A: number of saccades, B: duration of fixation, C: amplitude of saccades, D: coefficient of variation (CV) of saccade amplitude, E: number of repeated fixations, F: instability ratio of fixation. The bars show the values of mean and standard error. Grey bars are for SCA patients and white bars for normal subjects. The number of saccades per second and duration of fixation in SCA patients were identical to those in normal subjects for both 4- and 48-item tasks. Amplitude of saccades was smaller in SCA patients than in normal subjects for both 4- and 48-item tasks, although these differences were not statistically significant. CV of saccade amplitude was larger in SCA patients than in normal subjects only in the 4-item task. Number of repeated fixations and instability ratio of fixation were larger in SCA patients than in normal subjects for both 4- and 48-item tasks.

doi:10.1371/journal.pone.0116181.g009

$F_1=5.450$, $p=0.026$). Similar re-fixations would also occur when the subjects were processing the distractors (see the analysis of oculomotor trajectory, Figs. 6 and 7). Of course, it must be noted that it is technically difficult to differentiate between 'meaningful' and 'meaningless' re-fixations.

As noted above, impaired gaze fixations, interrupted by slow drifts of gaze preceded by saccades, can also impair visual processing of items. The instability ratio of fixation, i.e. the proportion of time occupied by such impaired fixation, was significantly larger in SCA patients than in normal subjects (Fig. 9F), implying unstable ocular fixation in SCA patients (tests of within-subjects effects: number of items × subject-group interaction, $F_1=0.912$, $p=0.346$; tests of

between-subjects effects: $F_1=11.524$, $p=0.002$). The ratio did not change with the number of items in either group (test of within-subject effect: number of items, $F_1=2.218$, $p=0.146$).

To assess how saccadic dysmetria affected the spatial separation of the gaze from the target, the landing positions of the gaze was counted by setting the region of interest (a target Landolt figure) (Fig. 6). Postulating a range of central vision of 2° of radius (=R) around the direction of the gaze, we counted the number of fixations which landed near each target within a certain distance during the visual search. In the 48-item task, the number of fixations made within a distance of R around the target (captured with central vision) was larger in SCA patients than in normal subjects (3.2 ± 1.1 vs. 2.6 ± 0.8, respectively; $p=0.070$). Within a distance of 1.5R, the number was 5.7 ± 2.6 for SCA patients and 3.8 ± 1.2 for normal subjects ($p=0.010$). In the 4-item task, the number of fixations made within a distance of R was 1.8 ± 0.7 in SCA patients and 2.0 ± 0.6 in normal subjects ($p=0.368$), and within a distance of 2R, the number was 3.3 ± 1.3 in SCA patients and 2.8 ± 0.6 in normal subjects ($p=0.155$), with no significant difference between groups. Within the distance of 3R, however, the number was 4.2 ± 1.7 in SCA patients and 3.0 ± 0.6 in normal subjects ($p=0.011$). Thus, for both the 4- and 48-item tasks, the number of fixations around the target became larger for SCA patients as the distance from the target grew larger.

Discussion

Our study suggests that the impairment of top-down visual processing in SCA patients mainly results from: 1) saccadic dysmetria resulting in larger separation of the landing locations of the gaze from the target, 2) re-fixation of the target (and possibly of distractors), and 3) impaired fixation due to slow drifts of gaze associated with nystagmus.

Top-down visual scanning is markedly impaired in SCA

In this study, we compared the ability of SCA patients and normal subjects to perform top-down and bottom-up visual searches. Importantly, SCA patients needed a markedly longer search time than normal subjects in the serial search task. In contrast, SCA patients and normal subjects showed almost the same search times in the pop-out search task. Meanwhile, the response times in both the direction and color discrimination tasks were comparable between SCA patients and normal subjects. This reflects the fact that simple visual processing remains intact in SCA patients, due to the absence of eye movements. These findings suggest that SCA patients have problems searching for a target serially using a top-down attentional process, whereas scanning with bottom-up attentional process is not affected.

These results are consistent with a previous study in which search behavior was slower and less efficient in patients with cerebellar infarcts, especially for tasks

requiring serial processing [37]. However, this is the first study to show the impairment of top-down visual scanning in patients with cerebellar dysfunction using saliency maps. We also analyzed what caused this impairment of search in SCA patients by monitoring eye tracking during the performance of visual search tasks.

SCA patients must perform more saccades to detect a target with low saliency

Serial search time was longer in SCA patients than in normal subjects, suggesting that SCA patients have to make more saccades to detect a target due to the impairment of top-down visual processing. We explored the reason for the longer search time in SCA patients. The lack of difference in mean fixation duration between SCA patients and normal subjects excluded the possibility that SCA patients were not fixating long enough to extract sufficient information during each fixation. If anything, the mean duration of fixation tended to be longer in the SCA patients. Furthermore, in both the direction and color discrimination tasks, which test simple cognitive visual processing without eye movement, the discrimination times were comparable between SCA patients and normal subjects, suggesting that SCA patients retain the ability to judge the characteristic features of a Landolt figure. Therefore, the possibility of impaired simple visual processing in the absence of eye movements is less likely. The search time difference between SCA patients and normal subjects was much more prominent in the serial than in the pop-out task. These findings suggest that having to make more saccades during the course of visual search is strongly associated with the longer search time in SCA patients. This poses the question: Why do SCA patients make more saccades than normal subjects?

Mechanisms of impaired visual processing suggested by gaze trajectories

Analyses of gaze trajectories during the serial visual search task suggests that making saccades itself prevented SCA patients from recognizing the visual items (target and distractors) efficiently, and they had to make more saccades to "see them better". The most impressive result of the eye-tracking studies was that SCA patients frequently looked directly (within central vision) or relatively close to the items (target or distractors) outside central vision but within 5 degree of items, but still went past and away from them, and later returned to the items. What this suggests is that SCA patients could not somehow process the visual information of the items properly when they had to make eye movements, so that they needed a lot of repeated fixations to better perceive the items. These re-fixations are of special note because they indicate that SCA patients may be unable to properly process and interpret what they are seeing "on the first try".

Analyses of gaze trajectories showed that saccadic dysmetria resulted in scattering of gaze fixations around the target, with larger spatial separation from

the latter, hampering accurate visual perception of the target from distractors. In addition, during gaze fixation, the visual processing of items was substantially impaired by saccade drifts due to the slow phase of nystagmus or saccade dysmetria. This was often followed by corrective saccades or saccades representing the quick phase of nystagmus. Even when the gaze approached the target with central or parafoveal vision, saccadic dysmetria and impaired fixation disrupted the processing of items.

Impairment of serial search relative to pop-out search and the contribution of eye movements

Recently, it has been proposed that the cerebellum contributes to cognitive functions, including attention [1, 6, 50]. While spatial shifts of visual attention are strongly associated with saccades (overt attention), attentional shift can also be made without eye movements (covert attention). Previous papers, using tasks that separately addressed overt and covert attention, consistently report that disturbed overt but normal covert shifts of attention in cerebellar lesions [34, 35, 50]. Therefore, the findings of our study agree with these papers, in that the serial search task requiring sequential (top-down) visual processing of items and gaze movement was affected in SCA patients, whereas the pop-out (bottom-up) search task was not.

Importantly, we also found that gaze movements during visual search provide a relatively good explanation for how the visual impairment occurred. By contrasting the serial and pop-out tasks, we clearly showed how the spatial shifts of attention that occur along with the gaze movements may impair the detection a target. We also showed how saccadic dysmetria (predominantly saccadic hypometria), re-fixations and nystagmus play important roles in the abnormal top-down visual scanning in SCA patients, resulting in imprecise eye movements, which hamper precise visual processing of central vision.

It must be acknowledged that the analysis of gaze trajectory does not provide a definite explanation of how impaired oculomotor control relates to the impairment of top down visual processing as demonstrated by prolonged search time. Top down visual processing may consist of three components: 1) a strategic component that determines how the subjects deploy their attention over a presented display to process the items visually, 2) an oculomotor component that determines how the subjects plan or program their oculomotor movements based on #1, and 3) a cognitive component that processed the visual information received during fixation. These parts are probably not independent of one another. That is to say, how accurately the gaze captures the presented items and how precisely the visual information taken in during fixation would in turn affect the strategic part, i.e., how the subjects plan subsequent eye movements. The presence of re-fixations suggests that even when the eye movements are made accurately enough to capture the items with central vision, the gaze can return to it, which suggests a deficit in the strategic component or the cognitive component of top-down visual processing. On the other hand, saccadic dysmetria and

impaired fixation are believed to represent a deficit in the oculomotor component, which also affects cognitive processing by hampering the incoming visual information [19].

We must be careful, however, that it is not possible to conclude, based on the present results, whether the impairments of top-down visual scanning are only due to deficits in eye movements control or are the consequence of a specific problem in top down mechanisms. To solve this problem, we would need visual search tasks that requires top down mechanisms to be performed, only with attentional shifts but without eye movements [51].

Conclusions

Using saliency maps, we showed that top-down visual scanning is impaired but bottom-up visual scanning remains intact in hereditary pure cerebellar ataxia patients. Saccadic dysmetria, re-fixations, and nystagmus may play important roles in the impairment of top-down visual scanning in these disorders, hampering precise visual processing.

Author Contributions

Conceived and designed the experiments: SM HM HF RH ST YU YT. Performed the experiments: SM TF ME YT. Analyzed the data: SM HM YT. Contributed reagents/materials/analysis tools: HM HF ME RH ST YU YT. Wrote the paper: SM HM RH ST YU YT.

References

1. **Schmahmann JD, Sherman JC** (1998) The cerebellar cognitive affective syndrome. Brain 121: 561–579.
2. **Kelly RM, Strick PL** (2003) Cerebellar loops with motor cortex and prefrontal cortex of a nonhuman primate. J Neurosci 23: 8432–8444.
3. **Ramnani N** (2006) The primate cortico-cerebellar system: anatomy and function. Nat Rev Neurosci 7: 511–522.
4. **Kawai Y, Suenaga M, Watanabe H, Ito M, Kato K, et al.** (2008) Prefrontal hypoperfusion and cognitive dysfunction correlates in spinocerebellar ataxia type 6. J Neurol Sci 271: 68–74.
5. **Suenaga M, Kawai Y, Watanabe H, Atsuta N, Ito M, et al.** (2008) Cognitive impairment in spinocerebellar ataxia type 6. J Neurol Neurosurg Psychiatry 79: 496–499.
6. **Schmahmann JD** (1991) An emerging concept. The cerebellar contribution to higher function. Arch Neurol 48:1178–1187.
7. **Andreasen NC, O'Leary DS, Cizadlo T, Arndt S, Rezai K, et al.** (1996) Schizophrenia and cognitive dysmetria: a positron-emission tomography study of dysfunctional prefrontal-thalamic-cerebellar circuitry. Proc Natl Acad Sci U S A 93: 9985–9990.
8. **Frings M, Maschke M, Timmann D** (2007) Cerebellum and cognition: viewed from philosophy of mind. Cerebellum 6: 328–334.
9. **Zee DS, Yee RD, Cogan DG, Robinson DA, Engel WK** (1976) Ocular motor abnormalities in hereditary cerebellar ataxia. Brain 99: 207–234.

10. **Vilis T, Hore J** (1981) Characteristics of saccadic dysmetria in monkeys during reversible lesions of medial cerebellar nuclei. J Neurophysiol 46:828–838.

11. **Noda H, Murakami S, Yamada J, Tamada J, Tamaki Y, et al.** (1988) Saccadic eye movements evoked by microstimulation of the fastigial nucleus of macaque monkeys. J Neurophysiol 60:1036–1052.

12. **Waespe W, Wichmann W** (1990) Oculomotor disturbances during visual-vestibular interaction in Wallenberg's lateral medullary syndrome. Brain 113: 821–846.

13. **Robinson FR, Straube A, Fuchs AF** (1993) Role of the caudal fastigial nucleus in saccade generation. II. Effects of muscimol inactivation. J Neurophysiol 70: 1741–1758.

14. **Takagi M, Zee DS, Tamargo RJ** (1998) Effects of lesions of the oculomotor vermis on eye movements in primate: saccades. J Neurophysiol 80: 1911–1931.

15. **Barash S, Melikyan A, Sivakov A, Zhang M, Glickstein M, et al.** (1999) Saccadic dysmetria and adaptation after lesions of the cerebellar cortex. J Neurosci 19:10931–10939.

16. **Büttner U, Grundei T** (1995) Gaze-evoked nystagmus and smooth pursuit deficits: their relationship studied in 52 patients. J Neurol 242: 384–389.

17. **Yabe I, Sasaki H, Takeichi N, Takei A, Hamada T, et al.** (2003) Positional vertigo and macroscopic downbeat positioning nystagmus in spinocerebellar ataxia type 6 (SCA6). J Neurol 250: 440–443.

18. **Suzuki Y, Kase M, Hashimoto M, Ohtsuka K** (2003) Leaky neural integration observed in square-wave jerks. Jpn J Ophthalmol 47: 535–536.

19. **Matsuda S, Matsumoto H, Furubayashi T, Fukuda H, Hanajima R, et al.** (2014) Visual scanning area is abnormally enlarged in hereditary pure cerebellar ataxia. Cerebellum 2014 Sep 18. [Epub ahead of print].

20. **Treisman AM, Gelade G** (1980) A feature-integration theory of attention. Cogn Psychol 12: 97–136.

21. **Duncan J, Humphreys GW** (1989) Visual search and stimulus similarity. Psychol Rev 96: 433–458.

22. **Treisman A** (1991) Search, similarity, and integration of features between and within dimensions. J Exp Psychol Hum Percept Perform 17:652–676.

23. **Nothdurft HC** (1993) The role of features in preattentive vision: comparison of orientation, motion and color cues. Vision Res 33:1937–1958.

24. **Ludwig CJ, Gilchrist ID** (2002) Stimulus-driven and goal-driven control over visual selection. J Exp Psychol Hum Percept Perform 28:902–912.

25. **van Zoest W, Donk M** (2004) Bottom-up and top-down control in visual search. Perception 33: 927–937.

26. **Land MF** (2009) Vision, eye movements, and natural behavior. Vis Neurosci 26: 51–62.

27. **Matsumoto H, Terao Y, Yugeta A, Fukuda A, Emoto M, et al.** (2001a) Where do neurologists look when viewing brain CT images? An eye-tracking study involving stroke cases. PLoS One 6: e28928.

28. **Treisman A** (1988) Features and objects: the fourteenth Bartlett memorial lecture. Q J Exp Psychol A 40: 201–237.

29. **Itti L, Koch C** (2001) Computational modelling of visual attention. Nat Rev Neurosci 2: 194–203.

30. **Koch C, Ullman S** (1985) Shifts in selective visual attention: towards the underlying neural circuitry. Hum Neurobiol 4: 219–227.

31. **Itti L, Koch C** (2000) A saliency-based search mechanism for overt and covert shifts of visual attention. Vision Res 40: 1489–1506.

32. **Foulsham T, Underwood G** (2008) What can saliency models predict about eye movements? Spatial and sequential aspects of fixations during encoding and recognition. J Vis 8:6.1–17.

33. **Foulsham T, Barton JJ, Kingstone A, Dewhurst R, Underwood G** (2009) Fixation and saliency during search of natural scenes: the case of visual agnosia. Neuropsychologia 47: 1994–2003.

34. **Golla H, Thier P, Haarmeier T** (2005) Disturbed overt but normal covert shifts of attention in adult cerebellar patients. Brain 128: 1525–1535.

35. **Ignashchenkova A, Dash S, Dicke PW, Haarmeier T, Glickstein M, et al.** (2009) Normal spatial attention but impaired saccades and visual motion perception after lesions of the monkey cerebellum. J Neurophysiol 102: 3156–3168.

36. **Alexandre MF, Rivaud-Péchoux S, Challe G, Durr A, Gaymard B** (2013) Functional consequences of oculomotor disorders in hereditary cerebellar ataxias. Cerebellum 12: 396–405.

37. **Machner B, Sprenger A, Kömpf D, Heide W** (2005) Cerebellar infarction affects visual search. Neuroreport 16: 1507–1511.

38. **Gomez CM, Thompson RM, Gammack JT, Perlman SL, Dobyns WB, et al.** (1997) Spinocerebellar ataxia type 6: gaze-evoked and vertical nystagmus, Purkinje cell degeneration, and variable age of onset. Ann Neurol 42: 933–950.

39. **Ishikawa K, Watanabe M, Yoshizawa K, Fujita T, Iwamoto H, et al.** (1999) Clinical, neuropathological, and molecular study in two families with spinocerebellar ataxia type 6 (SCA6). J Neurol Neurosurg Psychiatry 67: 86–89.

40. **Owada K, Ishikawa K, Toru S, Ishida G, Gomyoda M, et al.** (2005) A clinical, genetic, and neuropathologic study in a family with 16 q-linked ADCA type III. Neurology 65: 629–632.

41. **Sato N, Amino T, Kobayashi K, Asakawa S, Ishiguro T, et al.** (2009) Spinocerebellar ataxia type 31 is associated with "inserted" penta-nucleotide repeats containing (TGGAA)n. Am J Hum Genet 85: 544–557.

42. **Folstein MF, Folstein SE, McHugh PR** (1975) "Mini-mental state". A practical method for grading the cognitive state of patients for the clinician. J Psychiatr Res 12: 189–198.

43. **Trouillas P, Takayanagi T, Hallett M, Currier RD, Subramony SH, et al.** (1997) International Cooperative Ataxia Rating Scale for pharmacological assessment of the cerebellar syndrome. The Ataxia Neuropharmacology Committee of the World Federation of Neurology. J Neurol Sci 145: 205–211.

44. **Matsumoto H, Terao Y, Furubayashi T, Yugeta A, Fukuda H, et al.** (2011b) Small saccades restrict visual scanning area in Parkinson's disease. Mov Disord 26: 1619–1626.

45. **Harel J, Koch C, Perona P** (2006) Graph-Based Visual Saliency. Proceedings of Neural Information Processing Systems (NIPS).

46. **Harel J.** A saliency implementation in MATLAB. Available: http://www.vision.caltech.edu/~harel/share/gbvs.php. Accessed 2014 December 9.

47. **Itti L, Koch C, Niebur E** (1998) A model of saliency-based visual attention for rapid scene analysis. IEEE Trans Patt Anal Mach Intell 20: 1254–1259.

48. **Jacobs RJ** (1979) Visual resolution and contour interaction in the fovea and periphery. Vision Res 19:1187–1195.

49. **Burr DC, Ross J** (1982) Contrast sensitivity at high velocities. Vision Res 22: 479–484.

50. **Haarmeier T, Thier P** (2007) The attentive cerebellum - myth or reality? Cerebellum 6: 177–183.

51. **Eckstein MP** (2011) Visual search: a retrospective. J Vis 11. pii: 14.

Cerebellum (2014) 13:323–330
DOI 10.1007/s12311-013-0536-1

ORIGINAL PAPER

Mesenchymal Stem Cells Ameliorate Cerebellar Pathology in a Mouse Model of Spinocerebellar Ataxia Type 1

Serina Matsuura · Anton N. Shuvaev · Akira Iizuka · Kazuhiro Nakamura · Hirokazu Hirai

Published online: 17 November 2013

Abstract Spinocerebellar ataxia type 1 (SCA1) is a progressive neurodegenerative disorder caused by the expansion of a polyglutamine tract in the ataxin-1 protein. To date, no fundamental treatments for SCA1 have been elucidated. However, some studies have shown that mesenchymal stem cells (MSCs) are partially effective in other genetic mouse models of cerebellar ataxia. In this study, we tested the efficacy of the intrathecal injection of MSCs in the treatment of SCA1 in transgenic (SCA1-Tg) mice. We found that intrathecal injection of only 3×10^3 MSCs greatly mitigated the cerebellar neuronal disorganization observed in SCA1 transgenic mice (SCA1-Tg mice). Although the Purkinje cells (PCs) of 24-week-old nontreated SCA1-Tg mice displayed a multilayer arrangement, SCA1-Tg mice at a similar age injected with MSCs displayed monolayer PCs. Furthermore, intrathecal injection of MSCs suppressed the atrophy of PC dendrites in SCA1-Tg mice. Finally, behavioral tests demonstrated that MSCs normalized deficits in motor coordination in SCA1-Tg mice. Future studies should be performed to develop optimal protocols for intrathecal transplantation of MSCs in SCA1 model primates with the aim of developing applications for SCA1 patients.

Keywords Mesenchymal stem cells · Motor coordination · Mouse · Purkinje cells · Spinocerebellar ataxia type 1 · Neurodegenerative disease · Ataxia

S. Matsuura · A. N. Shuvaev · A. Iizuka · K. Nakamura · H. Hirai (✉)
Department of Neurophysiology, Gunma University Graduate School of Medicine, 3-39-22 Showa-machi, Maebashi, Gunma 371-8511, Japan
e-mail: hirai@gunma-u.ac.jp

Introduction

Spinocerebellar ataxia type 1 (SCA1) is an autosomal-dominant disorder caused by the expansion of a CAG trinucleotide repeat in the coding region of the *Sca1* gene (which encodes the ataxin-1 protein (ATXN1)) [1] and is characterized by neurodegeneration in the central nervous system (CNS) and the peripheral nervous system (PNS) [2]. The disease begins with cerebellar ataxia and is often associated with other neurological signs such as pyramidal signs, ophthalmoplegia, and cognitive impairment [3]. To date, there is no effective approach for reversing the symptoms of SCA1 patients.

SCA1 model animals are good tools for the exploration of therapeutic strategies for SCA1, such as gene therapy and stem cell therapy. SCA1-Tg mice that express a transgene containing the ATXN1 sequence with an 82 CAG repeat expansion in cerebellar Purkinje cells (PCs) have been generated [4, 5]. In a study utilizing gene therapy to treat CNS pathology, intracerebellar injection of recombinant adeno-associated virus vectors expressing short hairpin RNAs for ataxin-1 reduced the characteristic ATXN1 inclusions in PCs, restored cerebellar morphology, and profoundly improved motor coordination in SCA1-Tg mice [6]. The above work was based on the idea that the level of the polyglutamine-expanded protein is one of the factors that contributes to disease severity. This idea has been further confirmed in another study showing that an attenuation of cytotoxicity was mediated by microRNA-mediated decreases in the polyglutamine-expanded ATXN1 [7].

Regarding stem cell therapy for SCA1, the injection of neural precursor cells (NPCs) derived from the subventricular zone into the cerebellar white matter of SCA1-Tg mice promotes the recovery of motor behavior and morphological improvement of PCs [8]. Similar to NPCs, mesenchymal stem cells (MSCs) have been studied for their potential clinical use

in the treatment of neurodegenerative disorders [9]. MSCs are defined as multipotent progenitor cells that can differentiate into mesenchymal lineage cells, such as osteoblasts, adipocytes, and chondrocytes, and into other cell lineages, such as glial cells and hepatocytes [10–12]. MSCs can easily be isolated from multiple sources that include umbilical cord blood, bone marrow, adipose tissue, and dental pulp [13–16]. However, the therapeutic potential of MSCs has not been studied in SCA1 model animals; however, MSCs have been tested in mouse models of other types of cerebellar ataxia. A previous study using the SCA2 mouse model demonstrated that the injection of MSCs into the cerebellar cortex ameliorates motor function deterioration by rescuing cerebellar PCs [17]. Similarly, intracerebellar transplantation of bone marrow-derived MSCs into the cerebellum improves the motor function of *Lurcher* mice, which are characterized by a spontaneous frameshift mutation in the δ2 glutamate receptor gene [18].

In this study, we investigated the utility of MSCs in the treatment of SCA1 with SCA1-Tg mice. We chose intrathecal injection as the administration route because this route requires a minimally invasive procedure that is readily applicable to patients.

Materials and Methods

Mice

SCA1-Tg mice (B05 line) on the FVB background [4] were kindly provided by Dr. Harry T. Orr of the University of Minnesota, Minneapolis, MN, USA. SCA1-Tg mice and wild-type (WT) mice with the same genetic background were used for the experiments. The experimental protocol was approved by the Institutional Committee of Gunma University. All efforts were made to minimize suffering and reduce the number of animals used. Mice were given intrathecal injections of MSCs at 5 weeks old. Five-week-old SCA1-Tg mice showed no signs of ataxia; however, the mice at this age could not improve their performance after repetitive rotarod training without a preexisting defect in rotarod performance [4, 5]. Morphologically, only subtle changes in the dendritic staining of PCs were observed in the mice at 6 weeks old. Then, the mice develop signs of neurological abnormality, as assessed by home cage behavior from at least 12 weeks of age [4, 5]. In parallel with the behavioral abnormality, disorganization of the PC layer and shrinkage of the dendritic arborizations begin at 13 weeks of age [4, 5]. Therefore, rotarod tests were performed at 10, 11, 12, 13, 14, 15, and 20 weeks of age (i.e., 5, 6, 7, 8, 9, 10, and 15 weeks after MSC transplantation) to test the therapeutic effect of MSCs. Finally, the mice were subjected to morphological analyses at 21–23 weeks of age.

Culture of MSCs

KUM10, a mesenchymal stem cell line generated from C57/B6 mouse bone marrow, was purchased from the RIKEN BioResource Center. The cells were cultured in M061101 medium containing 10 % fetal bovine serum and antibiotics (GP BioSciences, Yokohama, Japan) and maintained in 5 % CO_2 at 37 °C.

Labeling of MSCs with GFP

Lentiviral vectors expressing GFP under the control of the cytomegalovirus promoter were produced and titrated as described previously [19]. Two microliters of lentiviral vectors at a titer of 1.7×10^{11} transduction unit/ml were added to exponentially growing MSCs in 6-cm dishes (approximately 20 % density). The MSCs were further cultivated for 3 days before grafting into mouse brains.

Injection of MSCs into the Meninges Covering the Cerebellum

Mice were deeply anesthetized with ketamine hydrochloride (100 mg/kg) and xylazine hydrochloride (20 mg/kg) and were placed in a stereotaxic apparatus; MSCs were injected as previously described [20]. Briefly, a sagittal incision in the skin was made to expose the cranium. A small burr hole was carefully made at 0 mm lateral and 5 mm caudal to bregma, and the tip of a Hamilton syringe (Hamilton, Reno, NV, USA) was inserted through the dura into the meninges over the superior colliculus. The Hamilton syringe was attached to a micropump holder (UltramicroPump II; World Precision Instruments (WPI), Sarasota, FL, USA) that was operated by a microprocessor-based controller (Micro4; WPI). GFP-labeled MSCs (6×10^5 cells) suspended in 10 μl of the culture medium were injected at a rate of 300 nl/min.

Verification of the Penetration of MSCs into the Cerebellar Cortex

To verify that MSCs were properly loaded into the meningeal space and were not erroneously released under the meninges, the skull was removed 1 h after the injection while leaving the arachnoid and pia maters attached to the brain. The presence of GFP-labeled MSCs was confirmed using a fluorescent stereoscopic microscope (VB7010; KEYENCE, Osaka, Japan). Subsequently, the arachnoid and pia maters were removed, and the absence of MSCs was confirmed.

Three days after administration, parasagittal brain slices (50 μm in thickness) were prepared using a microslicer (VT100s; Leica, Wetzlar, Germany), and the presence of GFP-labeled MSCs inside the cerebellar tissue was determined.

Intrathecal Injection of MSCs

Deeply anesthetized mice were fixed on the stereotaxic apparatus. The suboccipital skin between the occipital bone and the cervical spine was incised, and the meninges covering the medulla oblongata were exposed. A 30-g disposable needle (BD, Franklin Lakes, NJ, USA) was inserted into the subarachnoid space. After evacuation of approximately 15 μl of cerebrospinal fluid, 3×10^3 MSCs suspended in 10 μl of the culture medium were injected over 1 min using a Hamilton syringe.

Whole Cell Patch Clamp for Biocytin Infusion

Parasagittal cerebellar slices (200 μm in thickness) were prepared, and whole cell patch clamp was performed as previously described [19]. Briefly, mice were deeply anesthetized by inhalation of isoflurane (3 %) and euthanized by decapitation. The whole brain was quickly dissected out and immersed for several minutes in an ice-cold solution containing 234 mM sucrose, 26 mM $NaHCO_3$, 2.5 mM KCl, 1.25 mM NaH_2PO_4, 11 mM glucose, 10 mM $MgSO_4$, and 0.5 mM $CaCl_2$ (pH 7.4 when bubbled with 95 % O_2 and 5 % CO_2). Parasagittal slices of the cerebellar vermis were obtained using a microslicer (ZERO1; Dosaka-EM, Kyoto, Japan). The slices were maintained in an extracellular solution containing 125 mM NaCl, 2.5 mM KCl, 2 mM $CaCl_2$, 1 mM $MgCl_2$, 1.25 mM NaH_2PO_4, 26 mM $NaHCO_3$, 10 mM D-glucose, and 0.1 mM picrotoxin. This solution was bubbled continuously with a mixture of 95 % O_2 and 5 % CO_2 at room temperature for at least 45 min before initiation of the experiments. For visualization of PC morphology, 0.5 % biocytin (Sigma-Aldrich, St. Louis, MO, USA) diluted in intracellular solution containing 130 mM K-gluconate, 4 mM KCl, 20 mM HEPES, 1 mM $MgCl_2$, 4 mM MgATP, 1 mM NaGTP, and 0.4 mM EGTA was passively infused through a patch pipette into whole cell-clamped PCs. The slices were subsequently fixed with 4 % paraformaldehyde. Following overnight fixation at 4 °C, the slices were rinsed in 0.1 M phosphate-buffered saline (PBS, pH 7.4; three times, 5 min each) and treated with PBS containing a streptavidin-Alexa 594 conjugate. After a 2-h incubation at room temperature, the slices were mounted and coverslipped with Fluomount/Plus (Diagonostic Biosystems, Pleasanton, CA, USA).

Quantitative Analyses of the Dendritic Areas and Spine Densities of Spines in Biocytin-Infused PCs

The slices treated with biocytin and a streptavidin-Alexa 594 conjugate and were analyzed using a confocal laser-scanning microscope (LSM 5 PASCAL, Carl Zeiss, Oberkochen, Germany). Cerebellar slices were scanned at 1-μm intervals in Z-stack mode to project the entire dendritic tree onto a planar image, which was scaled according to intensity from 0 to 255 arbitrary units (AU), with 0 as the minimum intensity and 255 as the maximum. Binary images of biocytin-infused PCs were obtained by thresholding the projected images (i.e., the areas brighter than 100 of the 255 AU were considered to be dendrites). The dendritic area was calculated using the IP Lab imaging software (Scanalytics, Inc., Fairfax, VA, USA). For quantitation of PC spines, 35 regions of PC dendrites (totaling 350 μm in length) were randomly selected and the number of spines originating from a 10-μm length of the dendritic shaft was determined.

Immunohistochemistry

Parasagittal brain sections (50 μm in thickness) were incubated with mouse monoclonal anticalbindin D-28 K (calbindin) (Swant, Marly, Switzerland) antibody overnight at 4 °C. Then the sections were incubated with Alexa Fluor 488-conjugated anti-mouse IgG (Invitrogen, Carlsbad, CA, USA) for 2 h at room temperature. The sections were washed three times with 0.1 M PBS, pH 7.4, for 5 min after each step. The slices were mounted using Fluomount/Plus (Diagnostic Biosystems, Pleasanton, CA, USA) and were analyzed using a confocal laser-scanning microscope (LSM 5 PASCAL).

Rotarod Tests

The motor coordination of the mice was assessed using a rotarod test with accelerating (5-min trials at 4–40 rpm) and constant speed (2-min trials at 20 rpm) protocols. The test was performed at 5, 6, 7, 8, 9, 10, and 15 weeks after MSC transplantation (i.e., 10, 11, 12, 13, 14, 15, and 20 weeks of age). The Rota-Rod treadmill (Muromachi kikai, Tokyo, Japan) consists of a gridded plastic rod (3 cm in diameter, 10 cm in length) flanked by two large round plates (57 cm in diameter). Mice were first tested using the accelerating protocol. After all mice had been placed on the rod that was rotating at a constant speed (4 rpm), the rod began continuously accelerating from 4 to 40 rpm over 300 s. After a 30-min interval, the mice were tested using a constant speed protocol. In each session, the mice were subjected to four rotarod trials. Mice that were able to stay on until the cutoff time were removed from the rotarod, and the maximum time was recorded. Between trials, the mice rested for 5 min. The times the mice spent on the rod were automatically measured, and the time averaged across four trials was used for statistical analysis.

Statistical Analysis

The values obtained are expressed as means±SEM. Statistical analyses of the differences between the groups were performed with one-way analyses of variance (ANOVAs) followed by Tukey's post hoc test using the R software statistical

package (www.r-project.org) or the Origin software. p values less than 0.05 were taken as statistically significant.

Results

MSCs Loaded into the Meninges Enter the Brain

Because it is extremely difficult to trace MSCs a long time after the intrathecal injection of only 3,000 MSCs, we applied the following indirect method to prove the entering of intrathecallly injected MSCs into the brain. Intrathecally injected MSCs should enter the brain via the subarachnoid space. We tested whether KUM10, a bone marrow-derived MSC cell line, injected into the meninges could pass through the pia mater and enter the brain tissue. To do this, we injected KUM10 cells into the meninges above the superior colliculus just rostral to the cerebellum in WT mice and determined whether the cells could be detected in the cerebellar cortex.

One hour after loading KUM10 cells into the meninges, the skull was removed, leaving the arachnoid and pia maters attached to the brain surface. We observed GFP-labeled MSCs on the arachnoid and pia maters (Fig. 1a, b). However, the cells were not detected after removal of the arachnoid/pia maters from the brain (Fig. 1c, d). These results clearly indicate that MSCs were actually loaded onto the arachnoid/pia maters and were not released under the meninges.

Three days after administration, we examined the distributions of GFP-labeled KUM10 cells in the brain. GFP-labeled MSCs were essentially confined to the cerebellum. In the cerebellum, GFP signals were detected in lobules 3, 4, 5, and 6 and in the spaces between the folia (Fig. 1e, f). Thus, KUM10 cells injected in the subarachnoid space entered the cerebellum.

MSCs Rescued the Neuronal Organization of Mutant PCs

Five-week-old B05 SCA1-Tg performed as well as control WT mice on the rotating rod during the four trials on the first day [5]. However, during the subsequent 3 days of trials, the performances of B05 mice were significantly worse than those of control wild-type animals [5]. This observation indicates that the transgenic mice did not have a pre-existing defect in performance on the rotating rod at 5 weeks old. Rather, these mice could not improve their performance after repetitive training. Consistently, the transgenic animals showed no clear signs of ataxia at this age, as shown by the lack of abnormalities in home cage behaviors and gait patterns [4, 5]. Furthermore, there were only subtle changes in the dendritic staining of the PCs of the B05 mice at 6 weeks of age [5]. Taken together, the ataxia of B05 mice does not become clear before 5 weeks of age, although cellular functional and/or metabolic impairments may already exist at this stage. Because we sought to start treatment during the presymptomatic stage, we intrathecally injected KUM10 MSC cells into SCA1-Tg mice at 5 weeks of age. We applied a single intrathecal injection of 3×10^3 MSCs into the mice. This dosage (1×10^5 cells/kg body weight of mice) is similar to that of a recent paper in which patients with multiple sclerosis received a single intrathecal injection (29.5×10^6 cells corresponding to approximately 5×10^5 cells/kg body weight) [21].

We determined the effect of MSCs on the neuronal architecture of the cerebellum and, in particular, the PCs because the ATXN1 protein with abnormally expanded polyglutamine is specifically expressed in the PCs of the SCA1-Tg mice used in this study. The cerebella of the SCA1-Tg mice at 21–23 weeks of age had ectopically located PC cell bodies that resulted in multilayer PC soma as evidenced by calbindin

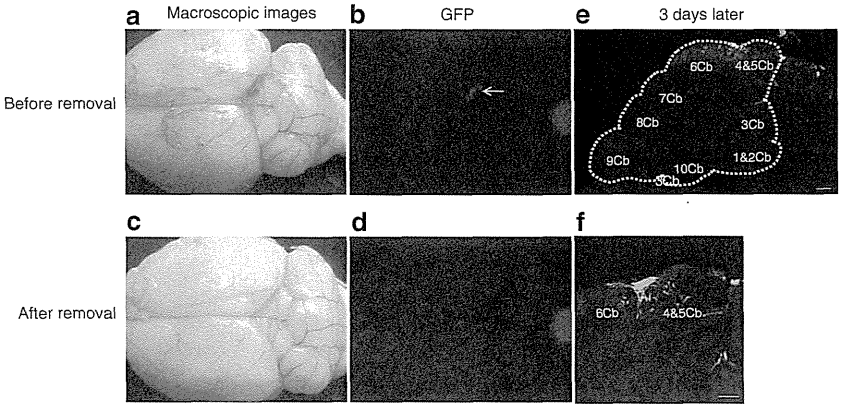

Fig. 1 MSCs loaded into the meninges enter the brain. GFP-labeled MSCs were stereotaxically injected into the meninges covering the superior colliculus. One hour after the injection, the brains were macroscopically (**a**, **c**) and fluorescently (**b**, **d**) observed before (**a**, **b**) and after (**c**, **d**) removal of the arachnoid/pia maters (**a–d**). Note that GFP-labeled MSCs were detected only before removal (*arrow*), indicating that the MSCs were actually loaded into the meninges not under the pia mater. Whether the MSCs in the meninges entered the brain tissue through the pia mater was examined via GFP signals in the sagittal sections of the MSC-injected mouse brains 3 days after the injection (**e**). GFP-positive MSCs in the cerebellum were found in lobule 3 (*3Cb*), lobule 4 and 5 (*4&5Cb*), and lobule 6 (*6Cb*) in magnified images (**f**). The *dotted line* indicates the area of the cerebellum. *Scale bars* 300 μm (**e**) and 200 μm (**f**)

immunostaining (Fig. 2a, b). Consistent with previous studies that have shown noticeable atrophy of the molecular layer in 15-week-old SCA1-Tg mice [5], calbindin staining also revealed a thin molecular layer in untreated SCA1-Tg mice (Fig. 2a, b). Notably, treated SCA1-Tg mice displayed a single layer of PC soma without ectopically located cell bodies and a molecular layer that was thicker than that of the untreated SCA1-Tg mice (Fig. 2a, b).

The thin molecular layer of the untreated SCA1-Tg mice is often associated with atrophy of PC dendrites. Indeed, when we injected biocytin into the PC soma to label individual PCs, most of the dendrites of the PCs of the untreated SCA1-Tg mice were shorter and less branched than those of the WT mice (Fig. 2c). This observation was confirmed by quantitative analysis of the areas occupied by each PC (Fig. 2d). PCs from WT mice had areas of 180±12 μm^2 (n=11 cells), whereas PCs from untreated SCA1-Tg mice had areas of only 43±7 μm^2 (n=9 cells; ANOVA, p<0.001). After treatment with MSCs, the SCA1-Tg mice exhibited a significant preservation of dendrites. MSC-injected SCA1-Tg mice had dendritic areas that were 2.5 times larger (105±11, n=13 cells) than those of untreated SCA1-Tg mice (ANOVA, p<0.001; Fig. 2d). Due to the smaller dendrites of the SCA1-Tg mice, we employed more detailed morphological analysis. The dendritic spines originating from the dendritic shafts worked as postsynapses. We quantified the density of the PC spines by counting the numbers of spines that originated from randomly-selected PC dendritic shafts 10 μm in length in the biocytin-infused PCs of the WTs, untreated SCA1-Tg and treated SCA1-Tg mice (n=35 regions each). The number of spines in the untreated SCA1-Tg mice (27.2±0.5) was significantly less than that of the WT mice (36.1±0.6; ANOVA followed by Tukey's post hoc test, p<0.001). Notably, injection of MSCs significantly increased the number of spines in the SCA1-Tg mice (32.1±0.9; ANOVA followed by Tukey's post hoc test, p<0.001; Fig. 2e, f).

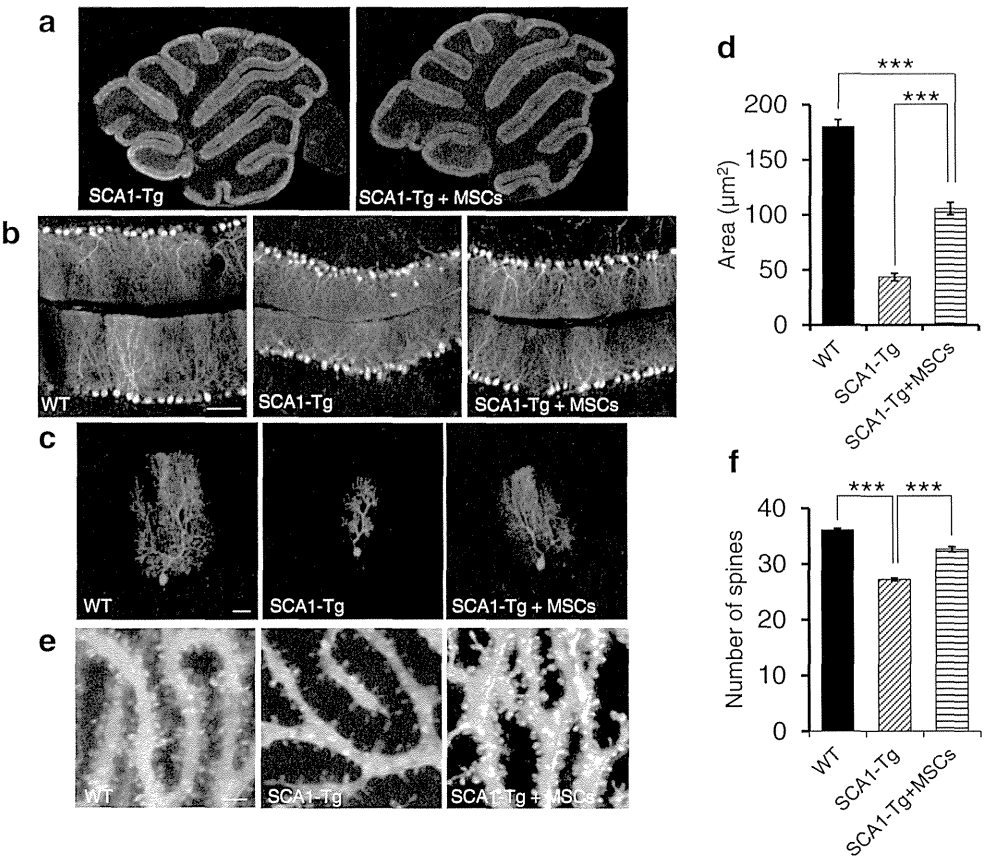

Fig. 2 Intrathecal injection of MSCs improved the morphology of the cerebellum of SCA1-Tg mice at 21–23 weeks old. Lower (**a**) and higher (**b**) magnifications of confocal images of calbindin-immunostained cerebellar slices from non-injected SCA1-Tg and MSC-injected SCA1-Tg mice (**a**) and WT mice (**b**). Dendritic morphologies of individual PCs of WT (n=11 cells), non-injected SCA1-Tg (n=9 cells), and MSC-injected SCA1-Tg mice (n=13 cells) (**c**, **d**). **c** Representative images of biocytin-injected PCs are shown. **d** The total dendritic area of the PCs was calculated using the IP Lab imaging software. The spine densities of individual PCs from the WT, non-injected SCA1-Tg and MSC-injected SCA1-Tg mice (n=35 regions each) (**e**, **f**). **e** Representative images of spines in biocytin-injected PCs are shown. **f** The total numbers of spines originating from the 10 μm long dendritic shafts of the biocytin-injected PCs were counted. The results are displayed as means±SEMs. ANOVA followed by Tukey's post hoc test, ***p<0.001. *Scale bars* 100 μm (**b**), 50 μm (**c**), and 2 μm (**e**)

Transplantation of MSCs Improved the Motor Phenotype of the SCA1-Tg Mice

Given the morphological preservation induced by MSC transplantation, we tested whether behavioral recovery would also be observed in treated SCA1-Tg mice. Motor coordination was repeatedly tested with the rotarod test from 5 weeks after the MSC transplant (10 weeks of age). In the accelerating protocol (Fig. 3a), the MSC-treated mice steadily improved their performance from 11 to 20 weeks of age. At 20 weeks of age, the MSC-injected group performed significantly better than the control SCA1-Tg group; the untreated SCA1-Tg mice stayed on the rod for ~120 s, whereas the MSCs-injected SCA1-Tg mice stayed on the rod for more than 200 s. The difference between WT, SCA1-Tg, and MSCs-injected SCA1-Tg mice was significant at 20 weeks of age (ANOVA, $F=7.1$; $p=0.005$). Tukey's post hoc tests revealed significant differences between the non-injected SCA1-Tg and the MSCs-injected SCA1-Tg mice at 20 weeks of age ($p=0.009$). In the constant speed protocol (Fig. 3b), significant differences were observed between the WT, SCA1-Tg, and MSCs-injected SCA1-Tg mice at 13, 14, and 20 weeks of age (ANOVA, $F=5.0$; $p=0.02$, $F=7.4$; $p=0.004$ and $F=7.8$; $p=0.003$, respectively). Tukey's post hoc tests revealed significant differences between the non-injected and the MSC-injected SCA1-Tg mice at 13 ($p=0.048$), 14 ($p=0.011$), and 20 weeks ($p=0.007$) of age.

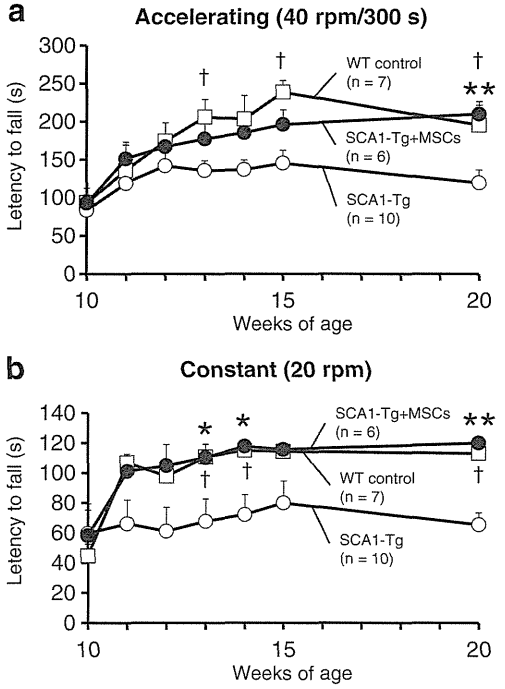

Fig. 3 Intrathecal injection of MSCs improved the motor behavior of SCA1-Tg mice. The motor coordination of the mice was tested with a rotating rod. Mice underwent eight trials per day on the accelerating (4–40 rpm) (**a**) and subsequent constant (20 rpm) (**b**) rotarod (four trials each) at 10, 11, 12, 13, 14, 15, and 20 weeks of age (i.e., 5, 6, 7, 8, 9, 10, and 15 weeks after MSC transplantation) (**a**, **b**). The rotarod performances of non-injected SCA1-Tg mice (SCA1-Tg control; $n=10$, two male and eight female mice) were compared with those of the MSC-injected SCA1-Tg mice (SCA1-Tg+MSCs; $n=6$, one male and five female mice) and non-injected WT mice (WT control; $n=7$, two male and five female mice). MSC-injected SCA1-Tg mice significantly improved their rotarod performances compared to the non-injected SCA1-Tg mice, which were not significantly different from the WT mice. The results are displayed as means±SEMs. ANOVA followed by Tukey's post hoc test; $*p<0.05$ and $**p<0.01$ for MSC-injected SCA1-Tg mice vs. non-injected SCA1-Tg mice, $+p<0.05$ for WT mice vs. SCA1-Tg non-injected mice

Importantly, the rotarod performances of the MSC-injected SCA1-Tg mice were not different from those of the WT mice at any of the tested weeks in either protocol (ANOVAs followed by Tukey's post hoc test, $p=1.00$, 0.90, 0.96, 0.53, 0.82, 0.24, and 0.87 in the accelerating protocol and $p=0.86$, 0.96, 0.94, 1.00, 0.98, 1.00, and 0.91 in the constant speed protocol at 10, 11, 12, 13, 14,15, and 20 weeks old, respectively) (Fig. 3a, b) suggesting that MSC grafting completely suppressed the progression of motor disturbances.

In a different set of experiments, we examined the influence of anesthesia, sham operations, and the injection of medium without MSCs using WT and B05 mice and confirmed that those treatments did not improve rotarod performance (data not shown).

Discussion

In the current study, we demonstrated that KUM10 MSCs injected into the subarachnoid space pass through the underlying pia mater, migrate into the cerebellar cortex, and exert therapeutic effects on SCA1 pathology. In past studies of MSC transplantation into mouse models of other types of cerebellar ataxia, authors have injected at least 10^5–10^6 cells [17, 18]. In our study, we injected only 3×10^3 MSCs into SCA1 model mice and observed clear motor and morphological improvements; these findings indicate that this small number of MSCs was highly effective. We observed improvement in rotarod performance that was sustained until 15 weeks after the injection of MSCs. Future studies with longer observation times will determine whether a decay in this effect occurs.

In a previous study of stem cell therapy for SCA1 [8], NPCs derived from the subventricular zone were injected into three sites (1×10^5 cells at each site) of the cerebellar white matter, and motor skills were evaluated in the same SCA1-Tg mice that were used in this study (the B05 line of SCA1-Tg) with a nearly identical accelerating rotarod protocol (4–40 rpm, four trials per day). Therefore, the comparison of these previous studies with our own provides valuable information regarding the optimal conditions for stem cell therapy for SCA1. The transplant of NPCs promotes the functional recovery and morphological improvement of PCs

at 24 weeks of age [8]. Although NPC grafting was effective for aged SCA1-Tg mice at approximately 24 weeks of age when significant PC loss had occurred, such treatment was not effective for the younger SCA1-Tg mice that were given the transplantation at 5 or 13 weeks. These observations suggest that NPCs specifically migrate toward substantially degenerated PCs (24 weeks old) and exert their therapeutic effects. Because we reasoned that it might be better to initiate stem cell therapy before any significant degeneration and loss of PCs occurred, we intrathecally injected MSCs at 5 weeks of age and observed a complete suppression of progressive motor deficits. Thus, MSCs, but not NPCs, may have the potential to target to less-degenerated PCs.

Human MSCs are known to secrete a variety of growth factors that have both paracrine and autocrine activities in the damaged brain [22]. MSCs target injured areas and release trophic factors that can suppress local inflammation, enhance angiogenesis, reduce free radical levels, inhibit fibrosis and apoptosis, and stimulate the recruitment, retention, proliferation, and differentiation of tissue-residing stem cells [23]. Although we have not yet identified the factor (or factors) that is secreted from MSCs to restore PC development, this factor is likely a neuron-specific trophic factor. Interestingly, a previous study suggested that few MSCs isolated from bone marrow fuse with the PCs of *Lurcher* ataxic mice [18], and most of these MSCs were located adjacent to the PC layer and expressed brain-derived neurotrophic factor, neurotrophin-3, or glial cell-derived neurotrophic factor; all of these neurotrophic factors are implicated in PC survival [18]. Thus, an attractive scenario is that intrathecally administered MSCs migrate toward degenerated PCs, make contact with PCs and directly provide neurotrophic factors to PCs to rescue them from degeneration. Although we wanted to prove this, we found that it was extremely difficult to identify the intrathecally injected 3,000 MSCs several months after the injection. Instead, in our preliminary experiment, we directly injected GFP-labeled MSCs into the cerebellar cortex, and found GFP-positive MSCs in close proximity to PC somas, suggesting trophic influence of the MSCs on adjacent PCs. Further study will prove how the MSCs rescue degenerating PCs of SCA1-Tg mice.

MSCs represent a promising tool in cell therapy and are currently being tested in Food and Drug Administration-approved phases I–III clinical trials for many disorders [24]. The cases of nervous system diseases that have received intrathecal injections of MSCs are accumulating. MSC therapy can improve/stabilize the course of progressive multiple sclerosis in the first year after injection with no serious adverse effects [21]. A recent paper reported that umbilical cord MSC injections into patients with spinal cord injuries were effective in 13 of 22 patients [25]. In most patients for whom treatment was effective, motor functions, sensory functions, or both were improved and bowel and bladder control abilities were improved. However, minor populations experienced headache (one case) or lower back pain (one case) during the intrathecal injection, and no treatment-related adverse events occurred during a follow-up periods that ranged from 3 months to 3 years [25]. Thus, MSCs are a potential treatment for SCA1 patients. However, the optimal number of intrathecally injected MSCs that maximizes therapeutic benefits and minimizes adverse reactions remains to be determined.

Conclusion

SCA1-Tg mice fail to improve their rotarod performance after repetitive training at 5 weeks of age and PC abnormalities, such as disorganization of the PC layer and shrinkage of the dendritic arborizations, beginning at 13 weeks of age. Intrathecal injection of only 3×10^3 MSCs in 5-week-old SCA1-Tg mice significantly suppressed the disorganization of the PC layer and the atrophy of dendritic arborization at 5 months of age and resulted in a maintenance of motor ability that was similar to that of wild-type mice as evidenced by behavioral analysis.

Acknowledgments This work was supported by the Funding Program for Next Generation World-Leading Researchers (LS021) (to H. Hirai) and by grants in aid from the Research Committee for Ataxic Disease, the Ministry of Health, Labour and Welfare of Japan (to K. Nakamura).

Conflicts of interest There are no potential conflicts of interest in the content of this paper.

References

1. Matilla-Dueñas A, Goold R, Giunti P. Clinical, genetic, molecular, and pathophysiological insights into spinocerebellar ataxia type 1. Cerebellum. 2008;7:106–14.
2. Robitaille Y, Schut L, Kish SJ. Structural and immunocytochemical features of olivopontocerebellar atrophy caused by the spinocerebellar ataxia type 1 (SCA-1) mutation define a unique phenotype. Acta Neuropathol. 1995;90:572–81.
3. Harding AE. Classification of the hereditary ataxias and paraplegias. Lancet. 1983;1:1151–5.
4. Burright NE, Clark BH, Servadio A, Matilla T, Feddersen MR, Yunis SW, et al. *SCA1* transgenic mice: a model for neurodegeneration caused by an expanded CAG trinucleotide repeat. Cell. 1995;82:937–48.
5. Clark HB, Burright EN, Yunis WS, Larson S, Wilcox C, Hartman B, et al. Purkinje cell expression of a mutant allele of SCA1 in transgenic mice leads to disparate effects on motor behaviors, followed by a progressive cerebellar dysfunction and histological alterations. J Neurosci. 1997;17:7385–95.
6. Xia H, Mao Q, Eliason LS, Harper QS, Martins HI, Orr TH, et al. RNAi suppresses polyglutamine-induced neurodegeneration in a model of spinocerebellar ataxia. Nat Med. 2004;10:816–20.
7. Lee Y, Samaco CR, Gatche RJ, Thaller C, Orr TH, Zoghbi YH. miR-19, miR-101 and miR-130 co-regulate ATXN1 levels to potentially modulate SCA1 pathogenesis. Nat Neurosci. 2008;11:1137–9.

8. Chintawar S, Hourez R, Ravella A, Gall D, Orduz D, Rai M, et al. Grafting neural precursor cells promotes functional recovery in an SCA1 mouse model. Neurobiol Dis. 2009;29:13126–35.
9. Mazzini L, Ferrero I, Luparello V, Rustichelli D, Gunetti M, Mareschi K, et al. Mesenchymal stem cell transplantation in amyotrophic lateral sclerosis: a phase I clinical trial. Exp Neurol. 2009;223:229–37.
10. Pittenger FM, Mackay MA, Beck CS, Jaiswal KR, Douglas R, Mosca DJ, et al. Multilineage potential of adult human mesenchymal stem cells. Sci. 2001;276:143–7.
11. Woodbury D, Reynolds K, Black BI. Adult bone marrow stromal stem cells express germline, ectodermal, endodermal, and mesodermal genes prior to neurogenesis. J Neurosci Res. 2002;69:908–17.
12. Lagasse E, Connors H, Dhalimy AM, Reitsma M, Dohse M, Osborne L, et al. Purified hematopoietic stem cells can differentiate into hepatocytes in vivo. Nat Med. 2000;6:1229–34.
13. Lee KO, Kuo KT, Chen MW, Lee DK, Hsieh LS, Chen HT. Isolation of multipotent mesenchymal stem cells from umbilical cord blood. Blood. 2004;103:1669–75.
14. Baddoo M, Hill K, Wilkinson R, Gaupp D, Hughes C, Kopen CG, et al. Characterization of mesenchymal stem cells isolated from murine bone marrow by negative selection. J Biochem. 2003;89:1235–49.
15. Gimble MJ, Guilak F. Adipose-derived adult stem cells: isolation, characterization, and differentiation potential. Cytotherapy. 2003;5:362–9.
16. Peneva M, Mitev V, Ishketiev N. Isolation of mesenchymal stem cells from the pulp of deciduous teeth. J IMAB. 2008;2:84–7.
17. Chang KY, Chen HM, Chiang HY, Chen FY, Ma HW, Tseng YC, et al. Mesenchymal stem cell transplantation ameliorates motor function deterioration of spinocerebellar ataxia by rescuing cerebellar Purkinje cells. J Biomed Sci. 2011;18:54.
18. Jones J, Merchán JJ, Bueno C, Pastor D, León VM, Martínez S. Mesenchymal stem cells rescue Purkinje cells and improve motor functions in a mouse model of cerebellar ataxia. Neurobiol Dis. 2010;40:415–23.
19. Shuvaev NA, Horiuchi H, Seki T, Goenawan H, Irie T, Iizuka A, et al. Mutant PKCγ in spinocerebellar ataxia type 14 disrupts synapse elimination and long-term depression in Purkinje cells *in vivo*. J Neurosci. 2011;31(40):14324–34.
20. Iwamoto N, Watanabe A, Yamamoto M, Miyake N, Kurai T, Teramoto A, et al. Global diffuse distribution in the brain and efficient gene delivery to the dorsal root ganglia by intrathecal injection of adeno-associated viral vector serotype 1. J Gene Med. 2009;11:498–505.
21. Bonab MM, Sahraian AM, Aghsaie A, Karvigh AS, Hosseinian MS, Nikbin B, et al. Autologous mesenchymal stem cell therapy in progressive multiple sclerosis: an open label study. Curr Stem Cell Res Ther. 2012;7:407–14.
22. Joyce N, Annett G, Wirthlin L, Olson S, Bauer G, Nolta AJ. Mesenchymal stem cells for the treatment of neurodegenerative disease. Regen Med. 2010;5:933–46.
23. Meyerrose T, Olson S, Pontow S, Kalomoiris S, Jung Y, Annett G, et al. Mesenchymal stem cells for the sustained in vivo delivery of bioactive factors. Adv Drug Deliv Rev. 2010;62:1167–74.
24. Olson DS, Pollock K, Kambal A, Cary W, Mitchell MG, Tempkin J, et al. Genetically engineered mesenchymal stem cells as a proposed therapeutic for Huntington's disease. Mol Neurobiol. 2012;45:87–98.
25. Liu J, Han D, Wang Z, Xue M, Zhu L, Yan H, et al. Clinical analysis of the treatment of spinal cord injury with umbilical cord mesenchymal stem cells. Cytotherapy. 2013;15:185–91.

Citation: Molecular Therapy — Methods & Clinical Development (2014) **1**, 14032; doi:10.1038/mtm.2014.32

www.nature.com/mtm

ARTICLE

Distinct transduction profiles in the CNS via three injection routes of AAV9 and the application to generation of a neurodegenerative mouse model

Fathul Huda[1,2], Ayumu Konno[1], Yasunori Matsuzaki[1], Hanna Goenawan[1,2], Koichi Miyake[3], Takashi Shimada[3] and Hirokazu Hirai[1]

Using single-stranded adeno-associated virus serotype 9 (ssAAV9) vectors containing the neuron-specific synapsin-I promoter, we examined whether different administration routes (direct cerebellar cortical (DC), intrathecal (IT) and intravenous (IV) injections) could elicit specific transduction profiles in the CNS. The DC injection route robustly and exclusively transduced the whole cerebellum, whereas the IT injection route primarily transduced the cerebellar lobules 9 and 10 close to the injection site and the spinal cord. An IV injection in neonatal mice weakly and homogenously transduced broad CNS areas. In the cerebellar cortex, the DC and IT injection routes transduced all neuron types, whereas the IV injection route primarily transduced Purkinje cells. To verify the usefulness of this method, we generated a mouse model of spinocerebellar ataxia type 1 (SCA1). Mice that received a DC injection of the ssAAV9 vector expressing mutant ATXN1, a protein responsible for SCA1, showed the intranuclear aggregation of mutant ATXN1 in Purkinje cells, significant atrophy of the Purkinje cell dendrites and progressive motor deficits, which are characteristics of SCA1. Thus, ssAAV9-mediated transduction areas, levels, and cell types change depending on the route of injection. Moreover, this approach can be used for the generation of different mouse models of CNS/neurodegenerative diseases.

Molecular Therapy — Methods & Clinical Development (2014) **1**, 14032; doi:10.1038/mtm.2014.32; published online 6 August 2014

INTRODUCTION

The cerebellum plays a crucial role in motor coordination, and impairment of the cerebellum results in cerebellar ataxia. The cerebellar cortex is subdivided into three layers: the molecular layer, the Purkinje cell (PC) layer and the granule cell layer. There are five principal morphologically and functionally distinct types of neurons in the cerebellar cortex: PCs, granule cells and three types of interneurons comprising stellate cells, basket cells and Golgi cells. Granule cells receive inputs from brain stem areas, such as the pontine and vestibular nuclei, and send axons, called parallel fibers, to the PCs. The three types of interneurons modulate excitatory transmission from granule cells to PCs in an inhibitory fashion. In addition to these five types of neurons, the cerebellar cortex has a large number of radial glia. These glia are a specific type of astrocyte called Bergmann glia, whose soma are localized in the PC layer and extend processes radially into the molecular layer. PCs receive one more excitatory input from neurons in the inferior olivary nucleus through the climbing fibers. PCs project out from the cortex and make inhibitory synapses onto neurons in the deep cerebellar nuclei (DCN).

PCs are highly susceptible to persistent adverse environmental exposure, vascular disorders and certain genetic defects.[1–4] Hereditary spinocerebellar ataxia (SCA) is one representative disease that causes the degeneration of PCs. Hereditary SCA is currently classified into more than 30 types based on the genetic mutation.[2] PCs are primarily affected in certain types of SCAs, such as SCA6, SCA7, SCA14, and SCA31, whereas more diverse regions, including the cerebellar nuclei, brainstem and spinal cord, are impaired in other types of SCAs, such as SCA1, SCA2, and SCA3.

Gene therapy is a promising therapeutic approach that has the potential to cure these diseases. Many preclinical studies using mouse models of SCA in combination with lentiviral[5,6] or adeno-associated virus (AAV)[7,8] vectors expressing therapeutic genes have been conducted. The aims of the studies were to decrease the levels of toxic mutant protein by enhancing degradation pathways[6,9,10] or suppressing translation via the expression of shRNAs[8] or miRNAs[11] directed at the mRNA of the mutant genes. In some studies, these interventions led to the amelioration of the disease phenotype in the mouse model of the disease.[6,8] However, as the mouse cerebellum is far smaller than that of humans, one challenge that must be met before proceeding to clinical trials is the expansion of the transduced areas of the cerebellum for PC-specific SCA types and broad transduction beyond the cerebellum to the brainstem and the spinal cord for SCA types that diffusely affect the CNS.

[1]Department of Neurophysiology, Gunma University Graduate School of Medicine, Maebashi, Japan; [2]Department of Physiology, Faculty of Medicine Universitas Padjadjaran, Bandung, Indonesia; [3]Department of Biochemistry and Molecular Biology, Nippon Medical School, Tokyo, Japan. Correspondence: H Hirai (hirai@gunma-u.ac.jp)
Received 24 March 2014; accepted 11 June 2014

AAV vectors have a smaller particle size than lentiviral vectors and diffuse more extensively throughout brain tissue.[12,13] In this study, we used single-stranded AAV (ssAAV) vectors because they have an advantage of approximately double the transgene capacity over self-complementary AAV (scAAV) vectors (5 kb versus 2.5 kbp).[14] Using ssAAV serotype 9 (ssAAV9) vectors, we examined three different injection routes of viral administration (directly into the cerebellar cortex, intrathecally into the cisterna magna (located immediately caudal to the cerebellum) and intravenously through the superficial temporal vein close to the eye), and then assessed the extent of transduction in the CNS and the types of cells transduced in the cerebellar cortex. Based on the results obtained from the three different routes of viral administration, we generated a SCA mouse model using a ssAAV9 vector expressing mutant ATXN1 (~5 kb), a protein responsible for SCA1, and evaluated the utility of this approach for the generation of mouse models of neurodegenerative diseases in terms of the behavioral phenotype and neuronal degeneration.

RESULTS

Distinct CNS expression profiles are dependent on the viral administration route

The ssAAV9 vectors expressing green fluorescent protein (GFP) were used to deliver a transgene into neurons in the brain. We used the enhanced neuron-specific synapsin I promoter with the minimal CMV promoter at the 3′ end as a promoter for transgene expression (Figure 1a), which was recently developed in our laboratory. Woodchuck hepatitis virus posttranscriptional regulatory element (WPRE) was placed in the main AAV plasmid downstream of the GFP gene, which helped to enhance the stabilization of the mRNA and eventually increased the expression levels of the transgene.[15] The ssAAV9 vectors were injected into the cerebellar cortex (direct cortical (DC) injection), the intrathecal space (IT injection) or the superficial temporal vein (IV injection) as illustrated in Figure 1b–d. We used 4-week-old mice for DC and IT injections and postnatal day 1 (P1) pups for IV injection because the transduction efficiency in the brain after IV injection decreases rapidly as mice mature.[12]

The mice were euthanized 2 weeks after DC or IT injection and 4 weeks after IV injection. Initially, the overall native GFP expression in the whole brains and spinal cords was examined under a fluorescent stereoscopic microscope, followed by the observation of the parasagittal sections of the brain. In the DC injected mice, we observed extremely high levels of GFP primarily in the cerebellum, whereas we observed almost no GFP fluorescence in the cerebrum, brainstem or spinal cord (Figure 2a–c). After IT injection into the cisterna magna, modest levels of GFP fluorescence were detected throughout the brain with exceedingly bright fluorescence in the spinal cord and lobules 9 and 10 of the cerebellum close to the viral injection site (Figure 2d–f). This result may have occurred because the ssAAV9 vectors infused into the cisterna magna and initially infected lobules 9–10, and then most remaining viral particles were pushed downward along the spinal cord by the cerebrospinal fluid draining from the 4th ventricle, which resulted in the efficient transduction of the spinal cord and sciatic nerves (Figure 2e). By contrast, IV injection caused weak and diffuse expression of GFP throughout the CNS, but with a relatively robust expression in the spinal cord and the sciatic nerves (Figure 2g–i).

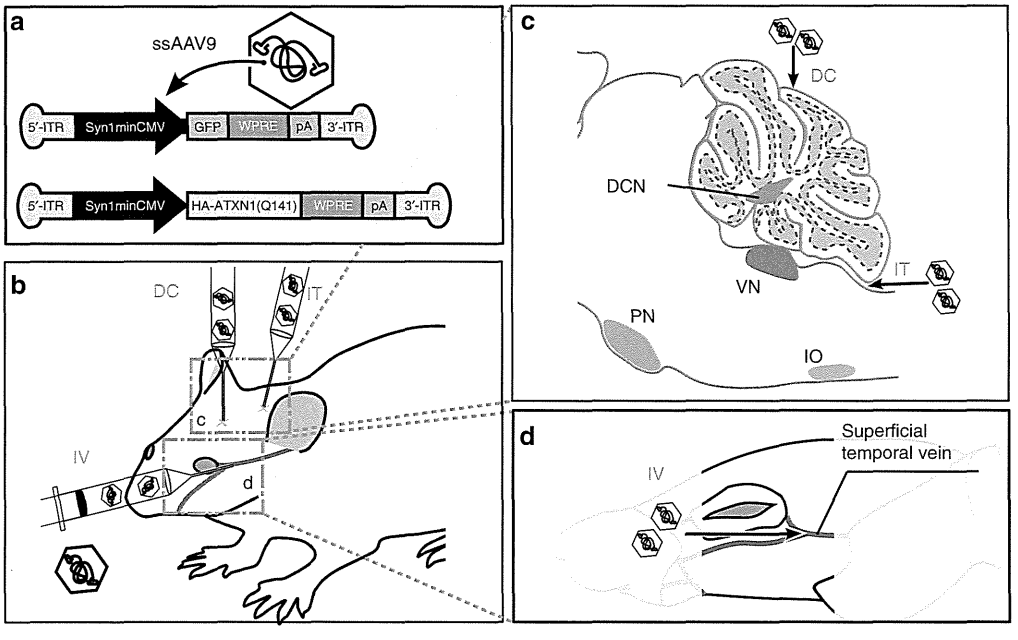

Figure 1 The ssAAV9 construct and a diagram showing the injection points. (**a**) Single-stranded adeno-associated virus serotype-9 (ssAAV9) DNA construct with its specific inverted terminal repeat (ITR) ends. We produced ssAAV9 vectors expressing the GFP under the control of the synapsin I promoter (Syn1) with the minimal CMV promoter at the 3′ end. Woodchuck hepatitis virus posttranscriptional regulatory element (WPRE) was placed downstream of the GFP gene. (**b**) Positions of the ssAAV9 vector injections relative to the mouse head. ssAAV9 vectors were injected directly into the cerebellar cortex (direct cortical (DC) injection), intrathecally into the cisterna magna (intrathecal (IT) injection) or into the superficial temporal vein (intravenous (IV) injection). (**c**) Illustration of a sagittal section of the cerebellum and brainstem showing the positions of the DC and IT injections. For DC injections, ssAAV9 vectors were injected into lobule 6. For IT injections, the vectors were administered into the cisterna magna. (**d**) The injection point for the IV route through the superficial temporal vein, which runs adjacent to the mouse eye. DCN, deep cerebellar nuclei; IO, inferior olivary nucleus; PN, pontine nuclei; VN, vestibular nuclei.

Broad GFP expression in the cerebellum after DC and IV, but not IT, injections

To examine the transduction profiles in the cerebellum, we made sagittal and transverse sections of the cerebellum and immunostained these sections for GFP and Nissl substance, a neuronal marker. The immunolabeled sections from mice that received DC or IV injections showed extensive transduction of the cerebellum that involved the entire vermal lobules (Figure 3a,g) and bilateral hemispheres (Figure 3b,h). We observed much higher GFP expression levels in the cerebella transduced by a DC injection than in those transduced by an IV injection (Figure 3a,b versus Figure 3e,f). The GFP expression resulting from a DC injection was centered on lobules 4–6 adjacent to the viral injection site (Figure 3a), while the highest expression levels produced by an IV injection were observed in lobule 10 (Figure 3e,g); this latter result most likely occurred because lobule 10 is immediately adjacent to the choroid plexus in which the cerebrospinal fluid containing the ssAAV9 particles is produced. By contrast, GFP expression produced by an IT injection was strong, but primarily confined to lobules 9 and 10 in the sagittal section (Figure 3c), which partly forms the ceil of the cisterna magna, *i.e.*, the subarachnoidal cavity into which the ssAAV9 vectors were injected. On the transverse section, GFP was inhomogeneously and sparsely expressed in the vermis and bilateral hemispheres by the IT injections (Figure 3d).

We quantitatively assessed the relative expression levels achieved by the three injection routes by measuring the GFP fluorescence intensity on the sagittal sections of the cerebellum (Figure 3i). The sagittal section was separated into four regions, including lobules 1–3, lobules 4–5, lobules 6–8, and lobules 9–10, as illustrated in Figure 3j. Overall, the DC injection route caused intense GFP expression throughout the entire lobules, whereas the IT and IV injection routes resulted in significantly weaker GFP expression in the whole lobules except lobules 9–10.

Efficient transduction of neuronal cells in the cortex and nuclei of the cerebellum

We next examined the cerebellar cell types transduced by the three different routes of viral administration. PCs, the sole output neurons from the cerebellar cortex, have large somata with well-differentiated dendrites and play critical roles in the processing of motor coordination. To examine the transduction of PCs, the cerebellar sections were double immunostained for GFP and Nissl substance or calbindin D-28K (calbindin), a PC marker. We observed that all three routes of vector administration produced an efficient transduction of PCs (Figure 4a,e,i, thick arrows), and this finding was confirmed by immunolabeling PCs with anti-calbindin antibody (Figure 4b,f,j, thick arrows).

The DCN are located in the white matter of the cerebellum and are the main relay from the cerebellar cortex. Neurons in the DCN receive inhibitory inputs from PCs and excitatory inputs from the brainstem nuclei through mossy and climbing fibers. We examined the transduction of neurons in the DCN in transverse sections immunostained for Nissl substance and GFP. We observed robust GFP expression in the large projection neurons (Figure 4c,d,g,h,k,l, arrows), but not the interneurons (Figure 4c,d,g,h,k,l, asterisks), in the DCN after all three routes of viral administration.

We quantitatively assessed the transduction efficiency of PCs by measuring the ratio of GFP-positive PCs to whole PCs in each lobular group (Figure 4m). The DC and IV injection routes transduced ~60–80% of PCs in the three lobular groups comprising the lobules 4–10, whereas the IT injection route transduced ~10% of PCs in most lobules (lobules 1–8) except one lobular group (lobules 9–10), which was adjacent to the IT injection site and attained a similar transduction efficiency (~60%) as the DC injection route. In summary, the analysis of the sagittal sections of the cerebellum revealed that 52%, 23%, and 62% of the PCs were transduced by the DC, IT, and IV injection routes, respectively.

Next, we studied in further detail the transduced cell types in the cerebellar cortex by double immunolabeling sections for GFP and parvalbumin, which is a marker for inhibitory neurons, S100, which is a marker for astrocytes, or NeuN, which is a marker for granule cells. Immunolabeling for parvalbumin showed that numerous stellate and basket cells expressed GFP in the slices infected by the DC and IT injection routes (Figure 5a,d, arrows) but not by the IV injection route (Figure 5g, arrows). No GFP expression was observed in Bergmann glia, which were immunostained for S100, in the slices infected by any of the administration routes (Figure 5b,e,h). In the granule cell layer, numerous granule cells, which were immunostained for NeuN, were transduced by the DC and IT injection routes (Figure 5c,f) but not by the IV injection route (Figure 5i). In any administration routes, GFP-expressing cells with relatively large

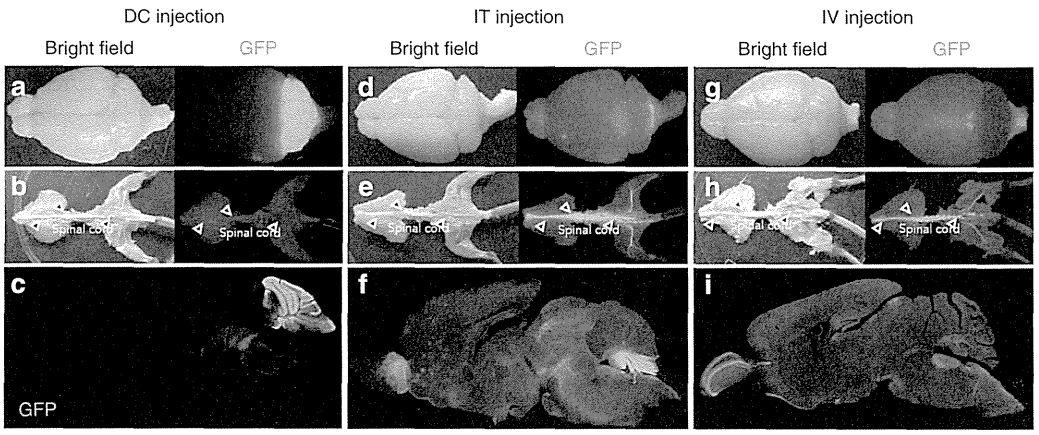

Figure 2 GFP expression profiles in the CNS resulting from the three different routes of administration of the ssAAV9 vector. Four-week-old mice received DC or IT injections of ssAAV9 vectors, while P1 mice received IV injections. The mice were sacrificed 2 weeks (DC and IT injections) or 4 weeks (IV injection) after the virus injection. Native GFP-fluorescent and bright field images of the brains and spinal cords are presented. (**a**–**c**) Mice that received DC injections. (**d**–**f**) Mice that received IT injections. (**g**–**i**) Mice that received IV injections. In each set of images, the upper, middle and lower images show the whole brains, spinal cords, and sagittal sections of the brain, respectively. The spinal cords are indicated by open arrowheads.

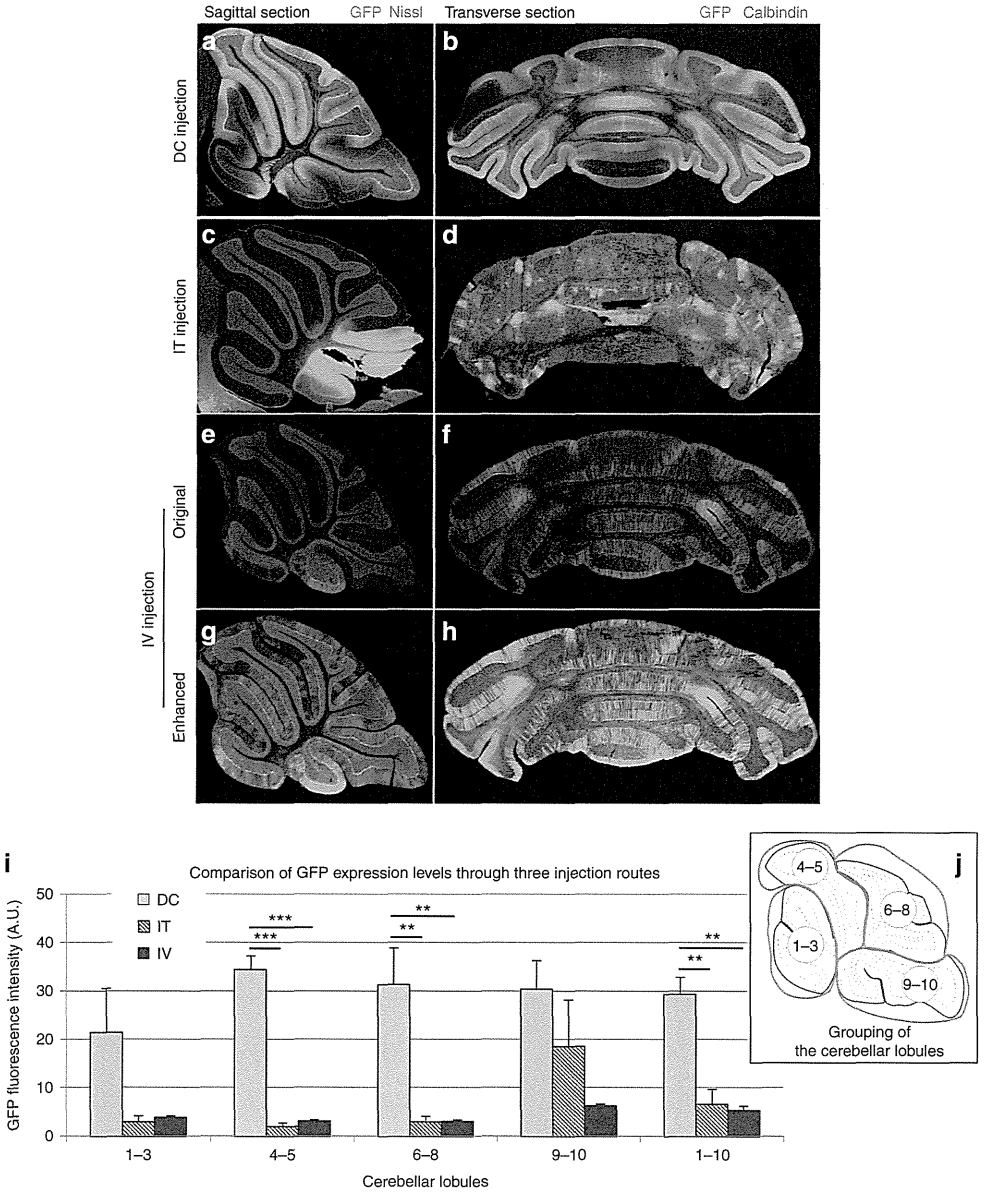

Figure 3 GFP expression profiles in the cerebellum resulting from the three different routes of administration of ssAAV9 vectors. (**a**,**b**) DC injection. (**c**,**d**) IT injection. (**e**–**h**) IV injection. Fluorescent images in the left and right rows are the sagittal and transverse sections of the cerebella, respectively, and were immunolabeled for GFP (green) and Nissl substance or calbindin (red). Images from (**a**) to (**f**) were acquired with same confocal laser strength, while images (**g**) and (**h**) were obtained with an enhanced laser intensity to make the transduction areas clearly visible. Note the wide-ranging transduction of the cerebellum that resulted from the DC and IV injections. Sagittal sections from mice that received IT injections showed high levels of GFP expression that were restricted to specific lobules (lobules 9 and 10). (**i**,**j**) Comparison of GFP expression levels through the three injection routes. Cerebellar lobules on a sagittal section of the cerebellar vermis were grouped into four parts, including lobules 1–3, 4–5, 6–8, and 9–10 as illustrated in (**j**). Each lobular group was traced, and the fluorescence intensity (arbitrary unit; A. U.) in each lobular group was measured using three slices from three mice in each group. Asterisks indicate statistically significant differences determined by one-way analysis of variance followed by Tukey's *post hoc* test, $^{**}P < 0.01$, $^{***}P < 0.001$.

somata and several processes were observed in the granule cell layer (indicated by asterisks in Figure 5c,i). Based on the morphology, these cells are considered to be Golgi cells.[16–18]

Transduction of neurons in the brainstem nuclei connected to the cerebellum

Neurons in the pontine (Figure 6a,d,g) and vestibular nuclei (Figure 6b,e,h) send mossy fibers to the cerebellar cortex, while neurons in the inferior olivary nucleus located in the medulla oblongata (Figure 6c,f,i) send climbing fibers to the DCN and PCs. Thus, we examined the transduction of neurons in these brainstem nuclei. Sections were immunolabeled for GFP and Nissl substance. The expression of GFP was observed in neurons in the pontine nuclei of slices transduced by any injection routes (Figure 6a,d,g). However, neurons in the vestibular nuclei and inferior olivary nucleus were selectively transduced by the IV injection route (Figure 6b,c,e,f,h,i, arrows).

Generation of a SCA1 mouse model by DC injection of ssAAV9 vectors expressing mutant ATXN1

To prove the utility of the present method for the production of SCA animal models, we used the DC injection route because the DC

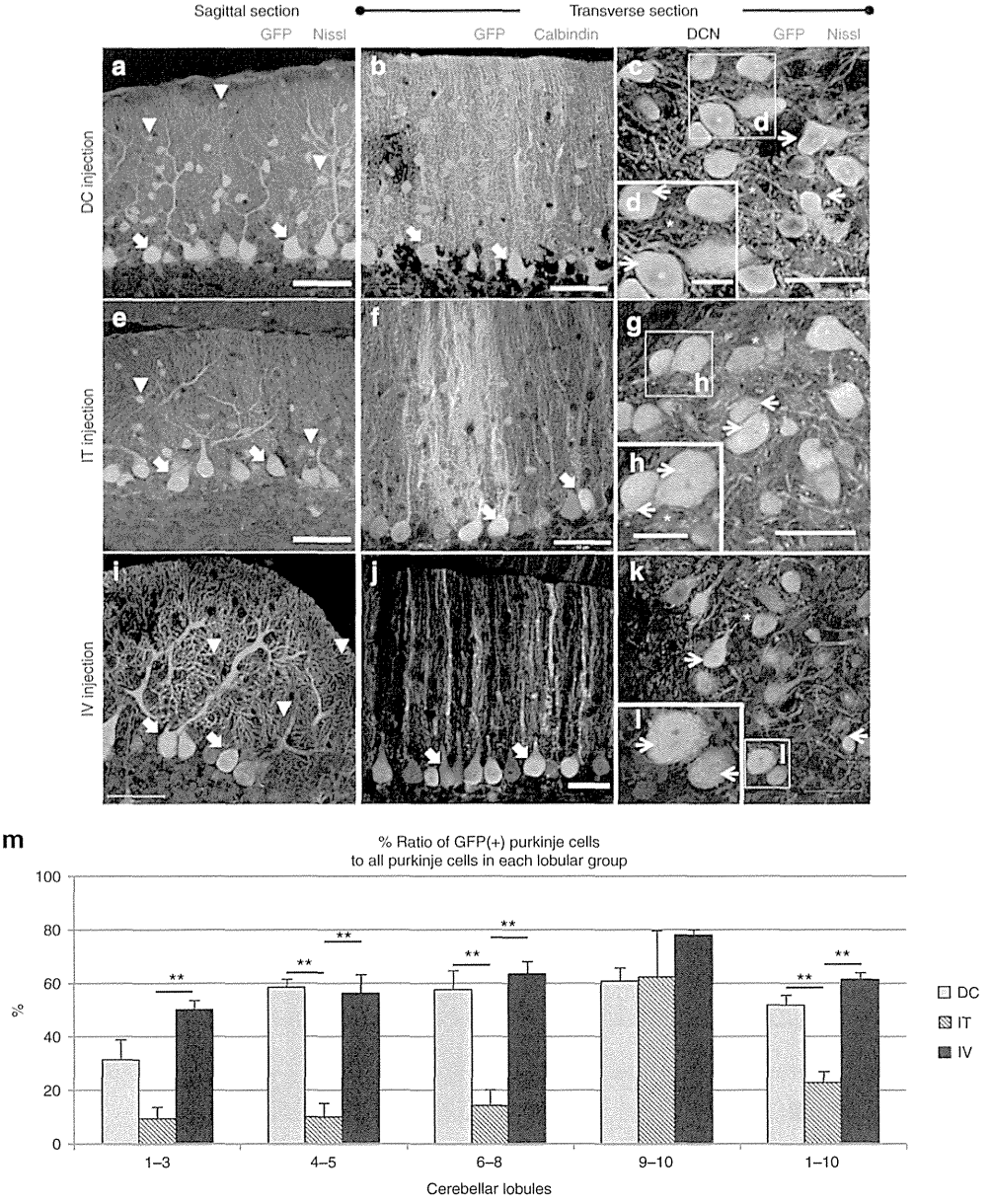

Figure 4 Neuron-specific transduction in the cerebellar cortex and deep nuclei resulting from all three routes of viral administration. Sagittal (left images) and transverse (middle and right images) sections of the cerebellum immunostained for GFP and Nissl substance (left and right images) or calbindin D-28K (calbindin) (middle images). (**a**–**d**) Sections from the mice that received DC injections. (**e**–**h**) Sections from the mice that received IT injections. (**i**–**l**) Sections from the mice that received IV injections. Arrowheads show interneurons, which were transduced only by DC and IT injections. Thick and thin arrows indicate transduced PCs and projection neurons in the DCN, respectively. Interneurons in the DCN, which are labeled by asterisks, were not transduced by any of the three administration routes. (**m**) Quantitative analysis of transduction efficacy of PCs by three injection routes. Graph shows the % ratio of the transduced PCs to all PCs were determined in four cerebellar groups as shown in Figure 3j. Each value was obtained from three slices/mouse using three mice in each viral injection group. Scale bars, 50 μm, except for panels (**d**,**h**,**l**) which are 20 μm. Asterisks indicate statistically significant differences determined by one-way analysis of variance followed by Tukey's *post hoc* test, $^{**}P < 0.01$.

injection of ssAAV9 vectors elicited efficient and robust transgene expression throughout the whole cerebellum (Figures 3i and 4m). Four-week-old C57BL/6 mice that showed approximately similar rotarod performances received a DC injection of ssAAV9 vectors expressing GFP or human influenza hemagglutinin (HA)-tagged ATXN1 with an abnormally expanded (141 repeats) polyglutamine stretch under the control of the enhanced synapsin I promoter (ssAAV9-Syn1minCMV-GFP-WPRE or ssAAV9-Syn1minCMV-HA-ATXN1(Q141)-WPRE). Sham-operated mice received a DC injection of a similar volume (10 μl) of phosphate-buffered saline (PBS). Three mouse groups (six mice each), *i.e.*, a PBS-injected group, a GFP-expressing group and a mutant ATXN1-expressing group, showed no statistically significant difference in rotarod performance until 4 weeks after the injection. However, the mutant ATXN1-expressing, but not the GFP-expressing, mice showed a significantly poorer performance than the control PBS-injected mice from 5 weeks after the injection (Figure 7a,b). The impaired performance of ATXN1-expressing mice became more evident thereafter and continued during the observation period (at least, up to 11 weeks after the injection). The weight of the mice did not change significantly